Monolayer-Protected Metallic Nanoparticles: Limitations of the Concentric Sphere Capacitor Model

Vladimir Garcia-Morales and Salvador Mafé*

Department de Física de la Terra i Termodinàmica, Universitat de València, E-46100 Burjassot, Spain

Received: November 29, 2006; In Final Form: March 28, 2007

Monolayer-protected clusters (MPC) having metallic core diameters of the order of 1 nm behave as multivalent redox molecules with small capacitances $C_{MPC} \approx 1$ aF. Theoretical estimations of this capacitance are usually based on the concentric sphere capacitor model. We have analyzed critically the predictions of this model over a broad range of experimental parameters: the metallic core radius r_0, the monolayer thickness d, the charge number z of the metallic core, the dielectric constant of the monolayer $\epsilon_{r,m}$, the base electrolyte concentration c_s, and the dielectric constant of the solvent $\epsilon_{r,s}$. To this end, we have solved the nonlinear Poisson−Boltzmann equation taking into account ion penetration. It is shown that the concentric sphere capacitance C_0 gives the correct order of magnitude as well as some qualitative features of the total MPC capacitance C_{MPC}, although significant deviations are obtained for realistic values of the above parameters, especially when ion and solvent penetration are important. The results obtained are compared with recent theoretical and experimental work by Murray et al. (*Anal. Chem.* **2005**, *77*, 2662), Girault et al. (*J. Phys. Chem. B* **2006**, *110*, 21460), and Quinn et al. (*J. Am. Chem. Soc.* **2003**, *125*, 6644) and provide some extensions of these previous studies.

1. Introduction

Monolayer-protected nanoclusters (MPC) with metallic core radius r_0 of the order of 1 nm behave as multivalent redox species with charge states separated by approximately constant electric potential differences.[1−6] The single electron transfer to and from the core leads to measurable electric potential changes because of the small MPC capacitance (approximately 1 aF). One of the most widely used theoretical approaches to estimate this capacitance C_0 is the concentric sphere capacitor model[4,5,7−24]

$$C_0 = 4\pi\epsilon_{r,m}\epsilon_0 r_0(r_0 + d)/d \quad (1)$$

where d is the monolayer thickness, ϵ_0 is the vacuum permittivity, and $\epsilon_{r,m}$ is the dielectric constant of the monolayer. Because r_0 and d are of the same order of magnitude, C_0 increases with the core radius and decreases with the monolayer thickness. The physical limits of C_0 correspond to a naked nanoparticle in a thick bulk dielectric medium for $r_0 \ll d$ and to a thin monolayer on a flat surface for $r_0 \gg d$.[7,8,25]

Despite its simplicity, eq 1 predicts correctly the order of magnitude of the experimental capacitances. However, the model is purely electrostatic and other effects should also be significant for a nanoparticle immersed in an electrolyte solution. Some assumptions underlying eq 1 are[17,25−27] (i) the MPC core is assumed to be spherical whereas the actual core shape could show other geometries (monodispersity is also implicitly assumed); (ii) the monolayer is characterized by a nonpenetrable region of dielectric constant $\epsilon_{r,m}$ and thickness d defined by the fully extended chains; and (iii) the monolayer/solution interface is assumed to be sharp, and the diffuse electrical double layer (EDL) in the solution is ignored. If the latter is not the case, the ions and solvent are assumed not to penetrate the monolayer, which defines then the distance of closest approach of the electrolyte ions to the MPC core. A few useful extensions to the above model have been considered recently.[25−27]

It is particularly important to quantify the effect of the solvent and electrolyte solution properties on the experimental values of C_{MPC} using the well established approaches of the electrochemical theory.[6,25−28] Girault and co-workers[25,29,30] considered the effect of organic solvents on the redox properties of the MPC both theoretically and experimentally, showing clearly that the potential separation between neighboring redox states increases with decreasing the relative permittivity (dielectric constant) of the solvent. In these studies, particular attention was paid to the correct dielectric description of the problem from an electrostatic viewpoint. The effect of the diffuse EDL in the solution was first ignored[29,30] and subsequently included[25] using the linear Poisson−Boltzmann (P−B) equation. Although this approximation may give some qualitatively correct results, it should be noted that typical nanoparticle surface potentials are approximately 1 order of magnitude higher than the thermal potential $RT/F \approx 26$ mV, where R, F, and T are the gas constant, the Faraday constant, and the thermodynamic temperature. Moreover, the linear P−B equation predicts capacitances and potential separations that do not depend on the charge number z, contrary to the predictions of the nonlinear equation that will be discussed here. Murray and co-workers[26] studied the nonlinear P−B equation approach proposed by Kontturi and co-workers,[6] paying special attention to the radial distribution of the diffuse EDL around small charged objects and comparing it with the planar electrode case (Gouy−Chapman theory).[16,26] The effects of solvent and ion penetration in the monolayer were also experimentally analyzed.

Quinn and co-workers have recently considered both theoretically and experimentally how the extent of ion penetration can be tuned by the core charge, the monolayer chain and solvent properties, and the electrolyte nature.[27] Counterions were

* Author to whom correspondence should be addressed. E-mail: smafe@uv.es.

10.1021/jp067920+ CCC: $37.00
Published on Web 05/04/2007

assumed to permeate the monolayer up to some distance from the core (a free parameter of the theory), and an analytical solution of the nonlinear P−B equation by Ohshima was used to obtain the electric potential in the resulting three region model.[27] However, this solution was originally derived for the case of a nonpenetrable spherical particle in free solution under the limiting case $a/L_D > 0.1$, where a is the sphere radius (the sum of the core radius and the monolayer thickness) and L_D is the solution Debye length.[31] The use of Ohshima's analytical solution for the radial heterostructure formed by the metallic core, the chain monolayer, and the adjacent electrolyte solution layer may be questionable, especially at low electrolyte concentrations (high Debye lengths). In an attempt to adapt this analytical solution to the different regions characteristic of the MPC and the solution, boundary conditions relevant to the problem and finite size corrections were included.[27] Reasonable explanations to the observed phenomena were given despite the fact that the distance of closest approach of the diffuse layer ions is difficult to assign.[25] This fitting parameter was allowed to be either constant or to change with the charge number and, in some cases, surprisingly large ion penetrations were obtained. Overall, the theoretical approach by Laaksonen et al.[27] was useful to interpret a comprehensive set of experimental data concerning different solvents and base electrolytes.

On the basis of the above recent studies,[25−27] we provide new insights by solving the nonlinear P−B equation[6,26,28] without resorting to approximate analytical solutions, both in presence and absence of ion penetration. This allows us to analyze critically the predictions of the concentric sphere capacitor model over a broad range of experimental parameters: the geometrical (lengths r_0 and d) and electrostatic (the charge number z of the metallic core and the monolayer dielectric constant $\epsilon_{r,m}$) characteristics of the MPC and the electrolyte solution properties (the base electrolyte concentration c_s and the solvent dielectric constant and $\epsilon_{r,s}$). Although alternative quantum−mechanical treatments are available,[32] it has been shown experimentally that the P−B model provides a useful qualitative picture of the ion distribution in the case of a spherical charged sparse brush.[33] Also, this model is usually employed in studies on the formation and stability of charged nanoparticles in solution.[34] The numerical solution of the P−B equation allows us to obtain: (i) the electric potential radial distribution ϕ(r) around the MPC for different electrolyte concentrations and solvent dielectric constants; (ii) the dependence of the total MPC capacitance C_{MPC} on the parameters r_0, d, z, $\epsilon_{r,m}$, c_s, and $\epsilon_{r,s}$ for a broad range of experimental values; (iii) the influence of the solution capacitance[26] C_s on the total capacitance C_{MPC}; (iv) the role of capacitances C_m (monolayer) and C_s (solution) in the determination of the potential separation $\Delta V = e/C_{MPC}$ (where e is the absolute value of the electron charge) between quantized double layer charging events; and finally (v) the effects of ion penetration on C_{MPC} and ΔV (a qualitative discussion of the results in ref 27 is also given). The theoretical results provide a comprehensive account of the limitations of the concentric sphere capacitor model. Since this model is widely used as a first approximation to the nanoparticle electrical properties in the chemical,[4,5,9,17,21,23] physical,[14,15,18] and engineering[20] literature, the results could be of interest to a broad audience.

2. Model Equations

Figure 1 shows a schematic view of the MPC in the bathing solution. The P−B equation has to be solved in the two-region model[6] for the cases of absence and presence of counterion penetration in the monolayer. In the first case, the Laplace equation

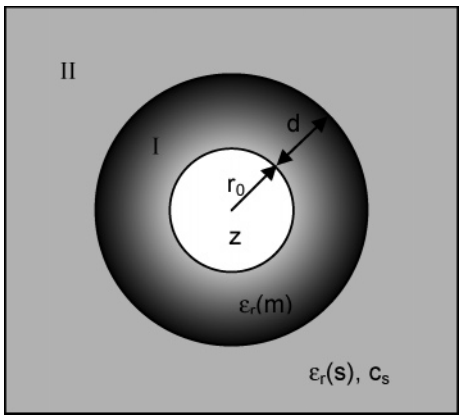

Figure 1. Schematic view of the MPC in the bathing solution. The P−B equation is solved in regions I (monolayer) and II (solution) for the cases of absence and presence of counterion penetration in the monolayer.

$$\frac{\partial^2\phi_m}{\partial r^2} + \frac{2}{r}\frac{\partial\phi_m}{\partial r} = 0, \qquad r_0 < r < r_0 + d \tag{2}$$

must be solved for the potential ϕ_m in region I, and the P−B equation

$$\frac{\partial^2\phi_s}{\partial r^2} + \frac{2}{r}\frac{\partial\phi_s}{\partial r} = \frac{2Fc_s}{\epsilon_{r,s}\epsilon_0}\sinh(F\phi_s/RT), \qquad r_0 + d < r < \infty \tag{3}$$

for the potential ϕ_s in region II. The appropriate boundary conditions are

$$-\epsilon_{r,m}\epsilon_0\left.\frac{\partial\phi_m}{\partial r}\right|_{r=r_0} = \frac{ze}{4\pi r_0^2} \tag{4a}$$

the continuity of the potential

$$\phi_m(r_0 + d) = \phi_s(r_0 + d) \tag{4b}$$

the continuity of the displacement vector at the monolayer/solution interface

$$\epsilon_{r,m}\left.\frac{\partial\phi_m}{\partial r}\right|_{r=r_0+d} = \epsilon_{r,s}\left.\frac{\partial\phi_s}{\partial r}\right|_{r=r_0+d} \tag{4c}$$

and the choice of the origin of potential

$$\phi_s(r\rightarrow\infty) = 0 \tag{4d}$$

From the electric potential drops across the radial coordinate, the total MPC differential capacitance can be obtained (see Figure 1) from

$$\frac{e}{C_{MPC}} = \frac{\partial\Delta\phi}{\partial z} = \frac{\partial}{\partial z}[\phi_m(r_0) - \phi_s(r\rightarrow\infty)] = \frac{\partial}{\partial z}\{[\phi_m(r_0) - \phi_m(r_0 + d)] + [\phi_s(r_0 + d) - \phi_s(r\rightarrow\infty)]\} \equiv \frac{e}{C_m} + \frac{e}{C_s} \tag{5}$$

Equation 5 defines the capacitances of the monolayer and the solution, respectively. Murray and co-workers[9,26] have experimentally analyzed the validity of the usual assumptions $C_s \gg C_m \approx C_0$ that lead to $C_{MPC} \approx C_0$ in eq 5.

As shown recently,[25] eqs 2−4 can be readily solved if the P−B equation (eq 3) is linearized:

$$\phi_m(r) = \frac{ze}{4\pi\epsilon_{r,m}\epsilon_0(r_0+d)}\left[\frac{\epsilon_{r,m}/\epsilon_{r,s}}{1+(r_0+d)/L_D}-1\right]+\frac{ze}{4\pi\epsilon_{r,m}\epsilon_0 r}, \quad r_0 < r < r_0+d \quad (6)$$

and

$$\phi_s(r) = \frac{ze}{4\pi\epsilon_{r,s}\epsilon_0[1+(r_0+d)/L_D]}\frac{e^{-[r-(r_0+d)]/L_D}}{r}, \quad r_0+d < r < \infty \quad (7)$$

Using eq 5, the potential distributions in eqs 6 and 7 lead to the capacitances[25]

$$C_m = 4\pi\epsilon_{r,m}\epsilon_0(r_0+d)(r_0/d) \equiv C_0 \quad (8)$$

$$C_s = 4\pi\epsilon_{r,s}\epsilon_0(r_0+d+L_D)[(r_0+d)/L_D] \quad (9)$$

From eqs 8 and 9, the total MPC capacitance is

$$C_{MPC} = \frac{C_m C_s}{C_m+C_s} = \frac{C_0}{1+\frac{\epsilon_{r,m}}{\epsilon_{r,s}}\frac{(r_0/d)}{[1+(r_0+d)/L_D]}} \quad (10)$$

Note that C_{MPC} does not depend on the metallic core charge number z in the linear approximation. Equation 9 shows that the diffuse EDL adds simply a second layer of concentration dependent thickness $L_D = [\epsilon_{r,s}\epsilon_0 RT/(2F^2c_s)]^{1/2}$ to the concentric sphere capacitor.[25] Differences between C_{MPC} and C_0 are significant in the cases $(r_0/d) \approx 1$ and $(r_0+d)/L_D < 1$ even for $\epsilon_{r,m}/\epsilon_{r,s} < 1$. Therefore, the assumption $C_{MPC} \approx C_0$ should be approximately valid for small metallic cores, high electrolyte concentrations, and no solvent penetration, especially in the limit $\epsilon_{r,m}/\epsilon_{r,s} << 1$.

Equation 2 should be modified to account for ion penetration. It has been shown experimentally that the metallic core charge, together with the chain characteristics and the electrolyte and solvent nature, dictate the monolayer permeability to ions.[26,27] In particular, counterions do not enter the monolayer without an electrostatic driving force between the core and bulk solution.[27] Therefore, we will concentrate on the electrical interaction between these ions and the core charge, allowing effective values for the monolayer dielectric constant to account indirectly for solvent penetration. The Laplace equation (eq 2) should then be replaced by the P−B equation

$$\frac{\partial^2\phi_m}{\partial r^2}+\frac{2}{r}\frac{\partial\phi_m}{\partial r} = -\frac{Fc_s}{\epsilon_{r,m}\epsilon_0}(K_+e^{-F\phi_m/RT}-K_-e^{F\phi_m/RT}), \quad r_0 < r < r_0+d \quad (11)$$

where K_i $(i = +,-)$ is the ionic partition coefficient between the solution and the monolayer (excluding the term for the electrical interaction of the ions with the metallic core charge that is explicitly accounted for in the exponentials of eq 11). Note that monolayer partition coefficients $K_i \ll 1$ should be expected because of the excluded volume effect due to the finite size of the monolayer chains[35] and the Born energy exclusion due to $\epsilon_{r,m} < \epsilon_{r,s}$.[27] These two terms counteract the electrostatic energy term in eq 11 that promotes counterion penetration. The partition coefficient K_i depends on the nature of the monolayer chains, the solvent and the base electrolyte: big counterions are expected to show lower values of K_i than small counterions, although the hydrophobic nature also matters.[25−27] The explicit estimation of the above contributions to K_i for each particular case constitutes a formidable problem[26,27,35] and, therefore, we will consider the partition coefficient to be a constant characteristic of the monolayer−solvent−electrolyte system. This permits a direct numerical solution of the P−B equation that shows the essential qualitative trends of the model for effective values of parameter K_i. For the sake of simplicity, a symmetrical base electrolyte is assumed first: the same partition coefficient K is introduced for the counterion and coion (note that the monolayer still selects the counterion over the coion because of the different sign of their charge numbers). Some results for the asymmetrical electrolyte case as well as a new theoretical approach to describe the effects of the compactness of region I on the counterion distribution will finally be included.

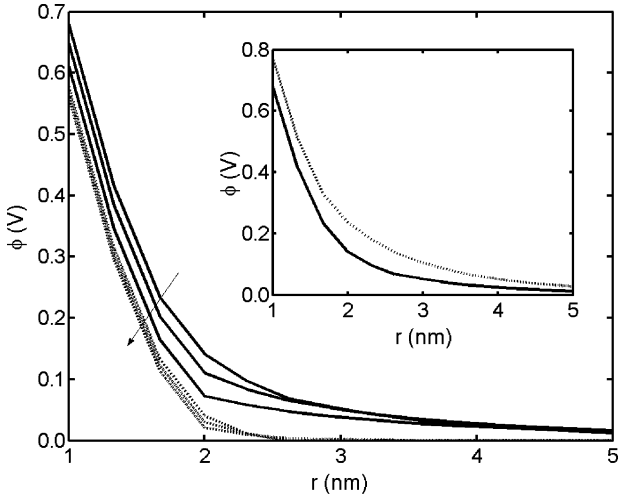

Figure 2. Electric potential radial distribution ϕ(r) around the MPC for the electrolyte concentrations $c_s = 1$ (continuous curves) and 100 mM (dotted curves). The arrow corresponds to increasing values of the solvent dielectric constant $\epsilon_{r,s} = 5$, 10, and 20. Other model parameters are $z = 3$, $r_0 = 1$ nm, $d = 1$ nm, and $\epsilon_{r,m} = 4$. The inset shows also ϕ(r) in the cases of the linear (dotted curve) and nonlinear (continuous curve) P−B equation for $c_s = 10$ mM and $\epsilon_{r,s} = 10$.

3. Results and Discussion

The above differential equations for the electric potential, subject to the respective boundary conditions, were solved numerically using the *Femlab 3.0* (Comsol AB, 2004) software package. Figures 2−11 (see also Figures S1−S3 in Supporting Information) give a survey of the results obtained under a broad range of experimental conditions. Figure 2 shows the electric potential radial distribution $\phi(r)$ around the MPC for the electrolyte concentrations $c_s = 1$ (continuous curves) and 100 mM (dotted curves). The arrow corresponds to increasing values of the solvent dielectric constant $\epsilon_{r,s} = 5$, 10, and 20 leading to lower potential drops in the solution layer, especially for the highest electrolyte concentration. Other model parameters are $z = 3$, $r_0 = 1$ nm, $d = 1$ nm, and $\epsilon_{r,m} = 4$. The inset shows also $\phi(r)$ in the cases of the linear (dotted curve) and nonlinear (continuous curve) P−B equation for $c_s = 10$ mM and $\epsilon_{r,s} = 10$. As expected, the potential obtained with the linear approximation is higher than that calculated in the nonlinear case. Although both curves are qualitatively similar, they lead to significantly different capacitances, as it is discussed later.

Figure 3 shows C_{MPC} versus the metallic charge number z for the electrolyte concentrations $c_s = 1$, 10, and 100 mM in the curves. Other model parameters are $r_0 = 1$ nm, $d = 1$ nm, $\epsilon_{r,m} = 4$, and $\epsilon_{r,s} = 10$. The concentric sphere capacitor

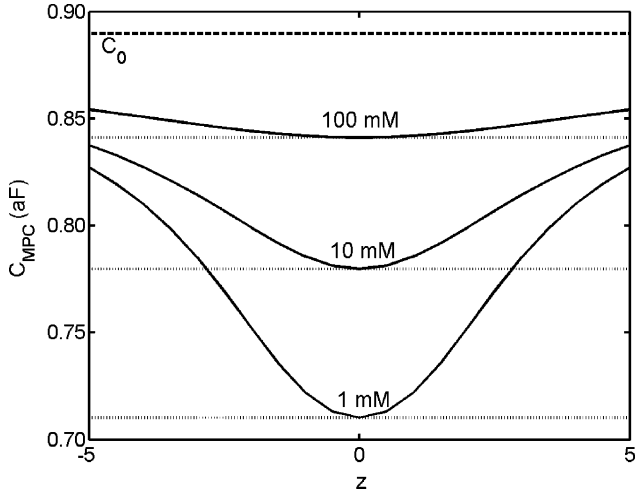

Figure 3. C_{MPC} vs z for the electrolyte concentrations $c_s = 1$, 10, and 100 mM in the curves. Other model parameters are $r_0 = 1$ nm, $d = 1$ nm, $\epsilon_{r,m} = 4$ and $\epsilon_{r,s} = 10$. The concentric sphere capacitor capacitance C_0 (dashed line, eq 1) and the total MPC capacitances obtained with the linear P−B equation (dotted curves, eq 10) are also included for comparison.

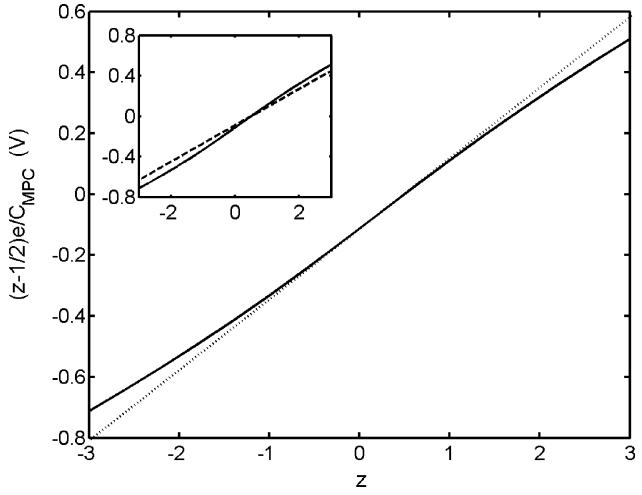

Figure 4. $(z - 1/2)e/C_{MPC}$ versus z for the electrolyte concentration $c_s = 1$ mM (continuous line). Other model parameters are $r_0 = 1$ nm, $d = 1$ nm, $\epsilon_{r,m} = 4$, and $\epsilon_{r,s} = 10$. The dotted straight line is included to better show the deviation from the linear behavior (constant C_{MPC}) that occurs at high charge numbers z. The inset shows also $(z - 1/2)e/C_{MPC}$ for the electrolyte concentrations, $c_s = 1$ (continuous line) and 100 (dashed line) mM.

capacitance C_0 (dashed line, eq 1) and the total MPC capacitance obtained with the linear P−B equation (dotted lines, eq 10) are also included for comparison. As expected for a classical model, the effect of the solution capacitance C_s on C_{MPC} is manifested by a symmetrical, significant dip in the capacitance C_{MPC} centered at $z = 0$.[26,28] The exact capacitance agrees with that obtained with the linear P−B equation (eq 10) only at low core charge numbers, showing that the linear solution has a limited validity. The increase of the capacitance from $z = 0$ is consistent with the dominance of the monolayer layer capacitance at very negative or positive potentials.[12] Remarkably, the capacitances C_{MPC} and C_0 differ by as much as 25% at low electrolyte concentrations. Also, the capacitance dip is still noticeable at high electrolyte concentrations, in qualitative agreement with ref 26, although the experimental dip is asymmetrical. The results of Figure 3 imply also that $\Delta V = e/C_{MPC}$ becomes larger at low electrolyte concentrations, an effect that should be

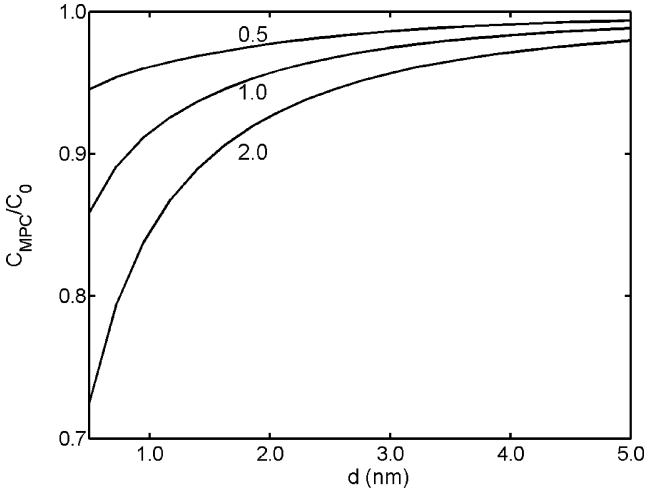

Figure 5. $C_{MPC}C_{MPC}/C_0$ versus the monolayer chain length d for the core radii $r_0 = 0.5$, 1, and 2 nm shown in the curves. Other model parameters are $z = 3$, $\epsilon_{r,m} = 4$, $\epsilon_{r,s} = 10$, and $c_s = 10$ mM.

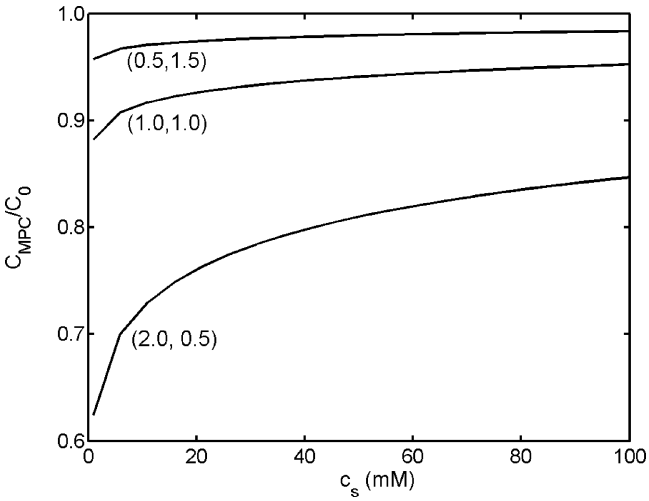

Figure 6. C_{MPC}/C_0 versus the electrolyte concentration c_s for the core radii and monolayer chain lengths (r_0, d) given in the curves (both lengths in nm). Other model parameters are $z = 3$, $\epsilon_{r,m} = 4$, and $\epsilon_{r,s} = 10$.

ascribed in part to changes in the diffuse EDL, as emphasized previously.[26]

Figure 4 shows the ratio $(z - 1/2)e/C_{MPC}$, which is related to the potential $\Delta V = e/C_{MPC}$ at which quantized double layer charging events occur,[2−4] versus z for the electrolyte concentration $c_s = 1$ mM (continuous line). Other model parameters are $r_0 = 1$ nm, $d = 1$ nm, $\epsilon_{r,m} = 4$, and $\epsilon_{r,s} = 10$. A plot of the formal potential characteristic of the MPC charging events versus the charge number z is linear provided C_{MPC} is constant, giving an average capacitance from the slope. This is indeed the case in the vicinity of the point of zero charge, although the potential separation becomes slightly nonuniform at more positive and negative potentials.[3,9,12,17] The experimental results are in qualitative agreement with the predictions of Figure 4 at high positive and negative charge numbers z (a dotted straight line is included to better show the deviation of $(z - 1/2)e/C_{MPC}$ from the linear behavior, constant C_{MPC}, eq 10). However, it should be mentioned that other effects (e.g., changes in the monolayer capacitance with z due to ion penetration and the particular density of the electronic states in the metallic core) can also be responsible for the observed deviation from linearity.[3,12,17] The inset in Figure 4 shows $(z - 1/2)e/C_{MPC}$ for the two electrolyte concentrations, $c_s = 1$ (continuous curves)

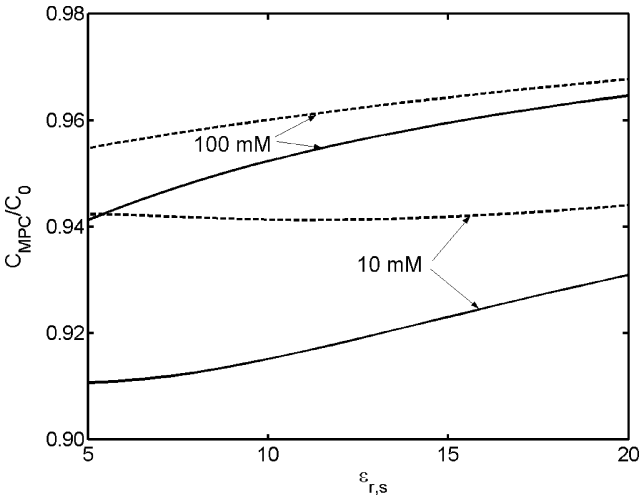

Figure 7. C_{MPC}/C_0 versus the solvent dielectric constant $\epsilon_{r,s}$ for the electrolyte concentrations $c_s = 10$ and 100 mM with the charge numbers $z = 3$ (continuous curves) and 5 (dashed curves). Other model parameters are $r_0 = 1$ nm, $d = 1$ nm, and $\epsilon_{r,m} = 4$.

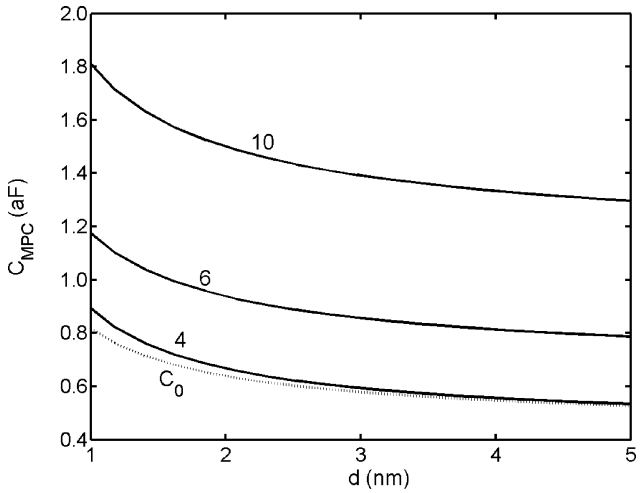

Figure 8. C_{MPC} (calculated with increasing values of $\epsilon_{r,m}$ to simulate solvent penetration) and C_0 (obtained with no solvent penetration for $\epsilon_{r,m} = 4$ in eq 1) versus the monolayer chain length d. Other model parameters are $z = 3$, $r_0 = 1$ nm, $\epsilon_{r,s} = 10$, and $c_s = 10$ mM.

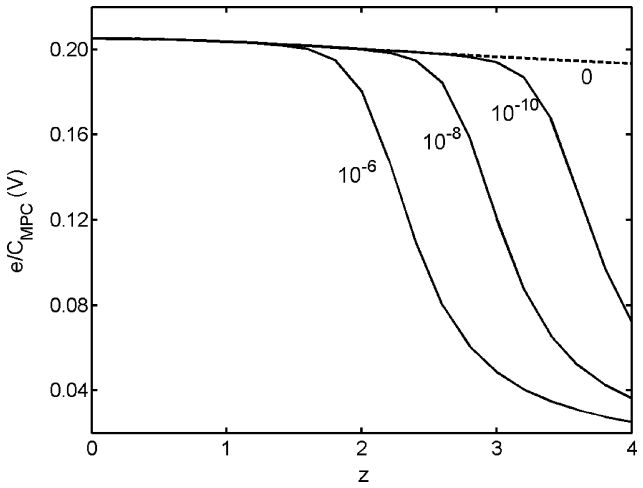

Figure 9. $\Delta V = e/C_{MPC}$ versus z for the partition coefficient values $K = 10^{-6}$, 10^{-8}, 10^{-10}, and 0 (dashed line, no ion penetration). Other model parameters are $r_0 = 1$ nm, $d = 1$ nm, $\epsilon_{r,m} = 4$, $\epsilon_{r,s} = 10$, and $c_s = 10$ mM.

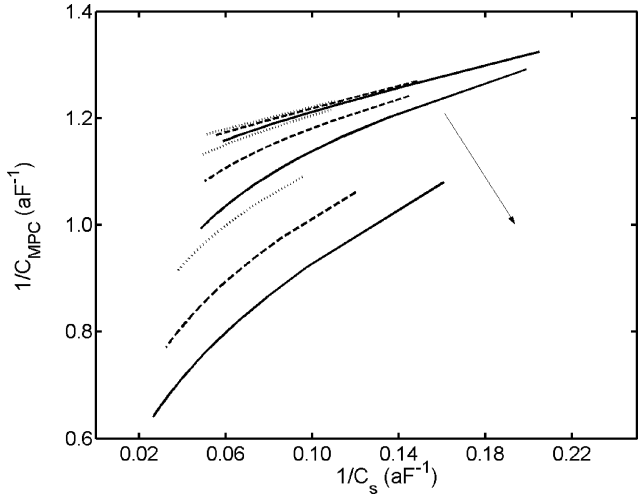

Figure 10. The inverse of the capacitance C_{MPC} versus the inverse of the solution layer capacitance C_s for $z = 2$ and $K = 10^{-7}$, 10^{-6}, and 10^{-5} (continuous curves); $z = 3$ and $K = 10^{-10}$, 10^{-9}, and 10^{-8} (dashed curves); and finally $z = 4$ and $K = 10^{-13}$, 10^{-12}, and 10^{-11} (dotted curves). In all cases, the arrow corresponds to increasing values of K. The values of $1/C_s$ in the horizontal axis correspond to electrolyte concentrations c_s in the range 1−100 mM. Other model parameters are $r_0 = 1$ nm, $d = 1$ nm, $\epsilon_{r,m} = 4$, and $\epsilon_{r,s} = 10$.

and 100 mM (dashed curves). This potential is not very sensitive to the electrolyte concentration in the immediate vicinity of $z = 0$.

Figure 5 shows C_{MPC}/C_0 versus the monolayer thickness d for the core radii $r_0 = 0.5$, 1, and 2 nm. Other model parameters are $\epsilon_{r,m} = 4$, $\epsilon_{r,s} = 10$, and $c_s = 10$ mM. The lower limit of r_0 is included here only to show the trends of the model, because at sufficiently small size the cluster develop molecule-like redox behavior.[2] The exact results are in qualitative agreement with the predictions of eq 10: the deviations of C_{MPC} from C_0 increase with decreasing d, being more significant at high core radii. Remarkably, the experimental capacitances (C_{MPC}) obtained from the formal potential characteristic of the nanoparticle charging steps appear to be consistently lower than those estimated from the spherical concentric capacitor model (C_0) for the data in Table 2 of ref 8. Figure 6 shows the ratio C_{MPC}/C_0 versus the electrolyte concentration c_s for the core radii and monolayer chain lengths (r_0, d) given in the curves (both lengths in nm). Other model parameters are $z = 3$, $\epsilon_{r,m} = 4$, and $\epsilon_{r,s} = 10$. The exact capacitance C_{MPC} tends asymptotically to C_0 as the electrolyte concentration increases (and, therefore, the Debye length in eq 10 decreases), although the two capacitances show relative deviations up to 35% for large metallic cores and small monolayer thicknesses. These deviations show clearly the importance of the solution layer capacitance C_s at low electrolyte concentrations, except for the case of small metallic cores where the monolayer capacitance C_m still dictates the value of the total capacitance C_{MPC} irrespective of the value of c_s.

Figure 7 shows the ratio C_{MPC}/C_0 versus the solvent dielectric constant ϵ_r(s) for the electrolyte concentrations $c_s = 10$ and 100 mM in the curves. Two charge numbers, $z = 3$ (continuous curves) and 5 (dashed curves), are considered. Other model parameters are $r_0 = 1$ nm, $d = 1$ nm, and $\epsilon_{r,m} = 4$. The MPC capacitances increase with the solvent dielectric constant, as reported in Table 2 of ref 9. At each concentration c_s, $C_{MPC} \approx C_0$ for $\epsilon_{r,s} \gg \epsilon_{r,m} = 4$, in agreement with the results by Girault and co-workers.[25,29,30] Because $\Delta V = e/C_{MPC}$, the potential separation should increase with decreasing the dielectric constant of the organic solvent, as observed and explained previously by these authors using the linearized P−B equation.[25,29,30] (This equation gives, however, capacitances and potential separations

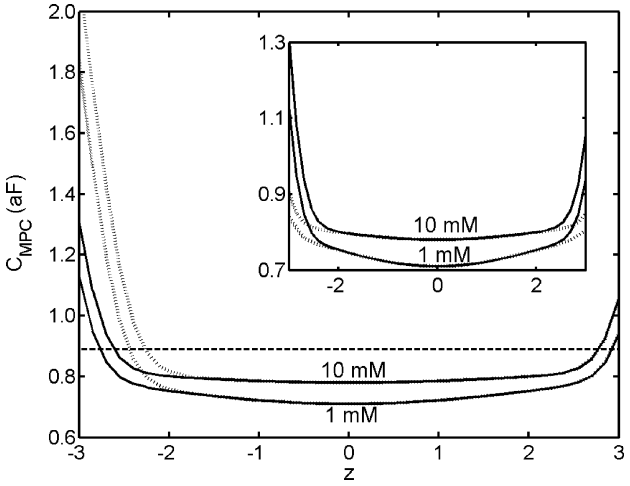

Figure 11. C_{MPC} versus z for the electrolyte concentrations $c_s = 1$ and 10 mM with $K_- = 10^{-8}$, in the cases $K_+ = 3K_-$ (continuous curves) and $K_+ = 30K_-$ (dotted curves). To better show the effect of the counterion inclusion on the asymmetry, the inset shows also the cases $K_- = 10^{-8}$ (continuous curves) and $K_- = 10^{-9}$ (dotted curves) for $K_+ = 3K_-$. Other model parameters are $r_0 = 1$ nm, $d = 1$ nm, $\epsilon_{r,m} = 4$, and $\epsilon_{r,s} = 10$. The concentric sphere capacitor capacitance (dashed line, eq 1) is also included for comparison.

that do not depend on the charge number z, contrary to the nonlinear P−B predictions of Figure 3.) The experimental choice of the solvent is determined usually by the joint solubility requirement of the MPC and the base electrolyte.[25] The results of Figure 7 may be relevant not only for a set of organic solvents with significantly different dielectric constants (or mixed solvents) but also for those cases where solvent penetration increases the effective value of $\epsilon_{r,m}$ in the monolayer.[25,26] Figure 8 gives the capacitances C_{MPC} (calculated with increasing values of $\epsilon_{r,m}$ to simulate solvent penetration) and C_0 (obtained with no solvent penetration for $\epsilon_r(m) = 4$ in eq 1) versus the monolayer chain length d. Other model parameters are $z = 3$, $r_0 = 1$ nm, $\epsilon_{r,s} = 10$, and $c_s = 10$ mM. Clearly, the effect of solvent penetration on C_{MPC} can be very significant (see also Figure S1 in Supporting Information) over a broad range of monolayer thicknesses d. Note also that C_{MPC} deviates from C_0 if d is small enough even when both capacitances are calculated with the same dielectric constant $\epsilon_{r,m} = 4$.

We consider next the case of ion penetration to the monolayer. As mentioned previously, the partition coefficient K must be very small because of the exclusion caused by the finite size of the ions[36,37] and monolayer chains[35] as well as the high Born-like energy barrier due to $\epsilon_{r,m} < \epsilon_{r,s}$.[27] These two exclusion effects prevent the counterion concentration in the monolayer to reach the unrealistically high values that would otherwise result because of the electrostatic energy in the Boltzmann exponential of eq 11. The above competing effects have to be taken into account in the estimation of reasonable values for K. The ratio between the average counterion concentration in the monolayer and the solution

$$\frac{\bar{c}_m}{c_s} = \frac{1}{(4\pi/3)[(r_0 + d)^3 - r_0^3]} \int_{r_0}^{r_0 + d} K e^{F|\phi_m|/RT} 4\pi r^2 dr \quad (12)$$

should not reach high values, therefore, because massive counterion penetration is not usually observed. Table 1 gives this ratio, calculated by numerical integration of the radial counterion profiles for different values of the partition coefficient K and the charge number z. Other model parameters are $r_0 =$ 1 nm, $d = 1$ nm, $\epsilon_{r,m} = 4$, $\epsilon_{r,s} = 10$, and $c_s = 10$ mM. Previous studies on ionic selectivity in confined geometries (e.g., an aqueous electrolyte solution within a charged pore, see ref 37 and references therein) appear to indicate that finite size corrections are very significant for concentrations close to 1 M. In our case, the size effects arise because of both the thiol chains and the relatively bulky counterions present in the monolayer. Therefore, the results in Table 1 suggests that an upper bound for the partition coefficient could be $K < 10^{-6}$ for $z = 3$, 4. This gives monolayer concentrations up to 0.1 M for the calculations in Table 1, which provides a conservative estimation for ion size corrections to be ignored. In this way, the finite size of the ions is taken into account indirectly, and the qualitative trends of the model can be discussed for different values of K without a detailed picture of the ion, solvent, and monolayer at the subnanometer scale. (The results obtained with a more elaborated model for the counterion distribution in region I will be given later.)

TABLE 1: The Ratio Between the Average Counterion Concentration in the Monolayer and the Electrolyte Concentration in the Solution (See Eq 12) for Different Charge Numbers z and Partition Coefficients K[a]

	c_m/c_s					
K	10^{-6}	10^{-7}	10^{-8}	10^{-9}	10^{-10}	10^{-11}
$z = 2$	0.10	0.011	0.0011	1.14×10^{-4}	1.14×10^{-5}	1.14×10^{-6}
$z = 3$	3.16	1.69	0.59	0.104	0.0115	0.0012
$z = 4$	8.35	6.55	4.80	3.14	1.67	0.57

[a] Other model parameters are $r_0 = 1$ nm, $d = 1$ nm, $\epsilon_{r,m} = 4$, $\epsilon_{r,s} =$ 10, and $c_s = 10$ mM.

Figure 9 shows the electric potential difference $\Delta V = e/C_{MPC}$ due to a single electron transfer versus the charge number z for the partition coefficients $K = 10^{-6}$, 10^{-8}, 10^{-10}, and 0 (dashed line, no ion penetration). Other model parameters are $r_0 =$ 1 nm, $d = 1$ nm, $\epsilon_{r,m} = 4$, $\epsilon_{r,s} = 10$, and $c_s = 10$ mM. The tail of the curve for $K = 10^{-6}$ in Figure 9 corresponds to z values giving exceedingly high counterion accumulations in the model (see Table 1), and is included only to show the limiting behavior. Significant decreases of e/C_{MPC} with z are predicted for reasonable values of K and z. The experimental data show indeed that ΔV decreases with the absolute value of z for the counterions that can penetrate the monolayer whereas it remains almost constant for those counterions that cannot penetrate this layer (the case $K = 0$ in Figure 9; see also Figure 2 of ref 27). In the latter case, the high excluded volume and hydrophobic barriers accounted for here by the partition coefficient K prevent counterion permeation. Figure 9 shows also that the potential $\Delta V = e/C_{MPC}$ can decrease with the absolute value of z for the nonlinear P−B equation even in the absence of ion penetration because C_{MPC} increases with z (see Figure 3). However, this is a rather small effect, as shown by the dashed curve corresponding to $K = 0$ in Figure 9, and it is counterion penetration that leads to significant decreases of ΔV with z, in agreement with the conclusions of Quinn et al.[27]

Figure 10 shows the inverse of C_{MPC} versus the inverse of C_s for $z = 2$ and $K = 10^{-7}$, 10^{-6}, and 10^{-5} (continuous curves); $z = 3$ and $K = 10^{-10}$, 10^{-9}, and 10^{-8} (dashed curves); and finally $z = 4$ and $K = 10^{-13}$, 10^{-12}, and 10^{-11} (dotted curves). The arrow corresponds to increasing K. The values of $1/C_s$ in the horizontal axis correspond to electrolyte concentrations c_s in the range 1−100 mM. Other model parameters are $r_0 = 1$ nm, $d = 1$ nm, $\epsilon_{r,m} = 4$ and $\epsilon_{r,s} = 10$. Clearly, deviations from the linear behavior (see Figure S1 in Supporting Information) are now obtained because of the counterion penetration, especially

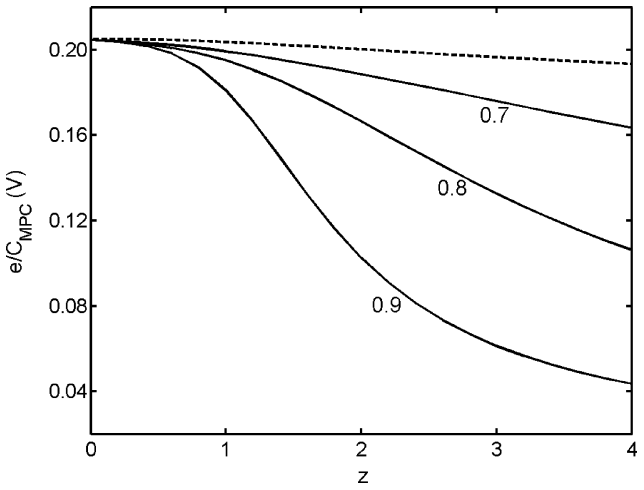

Figure 12. $\Delta V = e/C_{MPC}$ versus z for the partition coefficient $K = 10^{-2}$ with $q = 0.9$, 0.8, and 0.7 (continuous curves) in eq 13. The curve with $K = 0$ (dashed line, no ion penetration) is also shown. Other model parameters are $r_0 = 1$ nm, $d = 1$ nm, $\epsilon_{r,m} = 4$, $\epsilon_{r,s} = 10$, and $c_s = 10$ mM.

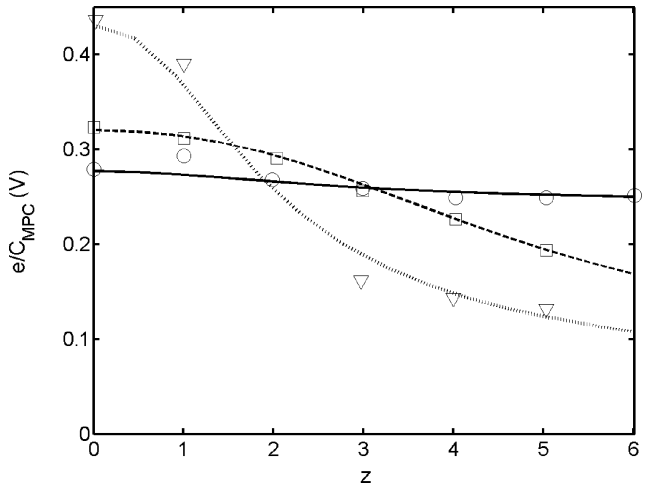

Figure 13. Experimental values (symbols) of $\Delta V = e/C_{MPC}$ versus z for $TPAsTPBF_{20}$ in DCE (circles), $TBAPF_6$ in DCE (squares), and $TBAPF_6$ in CB (triangles) (see ref 27 for details). The curves are obtained with eq 13 for the following partition coefficients and effective monolayer dielectric constants: $K = 0$ and $\epsilon_{r,m} = 3.6$ (continuous curve); $K = 10^{-3}$ and $\epsilon_{r,m} = 3.0$ (dashed line), and $K = 7 \times 10^{-3}$, and $\epsilon_{r,m} = 2.3$ (dotted line). Parameter $q = 0.79$ for the theoretical curves. The solution dielectric constants $\epsilon_{r,s} = 10.24$ (DCE) and 5.6 (CB), together with the characteristic values $r_0 = 0.81$ nm, $d = 0.77$ nm, and $c_s = 10$ mM, are taken from ref 27.

at high electrolyte concentrations c_s (these correspond to small values of $1/C_s$ in Figure 10).

Figure 11 shows the effect of the partition coefficient asymmetry on the C_{MPC} versus z curve (see also Figure S3 in Supporting Information) for the electrolyte concentrations $c_s =$ 1 and 10 mM, with $K_- = 10^{-8}$, for $K_+ = 3K_-$ (continuous curves) and $K_+ = 30K_-$ (dotted curves). To better show the effect of the counterion inclusion on the asymmetry, the inset shows also the cases $K_- = 10^{-8}$ (continuous curves) and $K_- = 10^{-9}$ (dotted curves) for $K_+ = 3K_-$. Other model parameters are $r_0 = 1$ nm, $d = 1$ nm, $\epsilon_{r,m} = 4$, and $\epsilon_{r,s} = 10$. The concentric sphere capacitor capacitance (dashed line, eq 1) is also included for comparison. The results show that significant deviations from the symmetric curves (see Figure S3 in Supporting Information) can occur because of the different nature of the respective counterion (the electrolyte cation for $z < 0$ and the electrolyte anion for $z > 0$). The asymmetry effects increase with increasing counterion inclusion (see inset). Remarkably, the difference between the cation and the anion of the base electrolyte need not be extreme to produce a noticeable asymmetry in the MPC capacitance.

In summary, the results of Figures 9−11 show that the effects of ion penetration are important at high charge numbers z, in qualitative agreement with experiments, although it should be mentioned that the observed capacitances could also reflect changes in the density of electronic states in the metallic core metallic not accounted for here. Moreover, assuming that the monolayer solution can be described by the P−B equation over all the range of z values might underemphasize the effects that the rigidity and compactness of this region exert on the counterion distribution. The incorporation of finite size effects in the diffuse electrical double layer of a free electrolyte solution is difficult[36] and this problem becomes even harder in the case of confined geometries (e.g., an aqueous electrolyte solution within a charged pore[37]). In our case, the size effects arise because of both the thiol chains and the counterions in the monolayer. An approximated procedure recently proposed to account for the ionic size is based an effective distance of closest approach of the counterion to the metallic core.[27]

In a final effort to extend the above model, we have considered a generalized P−B equation recently proposed for the study of charge correlations in the counterion distribution near to a macroion[38,39] and for the case of fractal phase spaces with reduced dimensionality.[40] In this approach, we consider the monolayer as a disordered medium where the thermal motion of the counterions is decreased because of electrostatic correlations and monolayer structural effects. The counterions can be in a range of states from frozen configurations where they are not able to move to diffuse configurations where the above P−B approach applies. The effect of the electrostatic correlations and the monolayer structure on the counterion distribution is accounted for by means of the Tsallis q-exponential distribution.[41] In terms of this distribution, the generalized P−B equation for the monolayer is[38−40]

$$\frac{\partial^2 \phi_m}{\partial r^2} + \frac{2}{r}\frac{\partial \phi_m}{\partial r} = \frac{FKc_s}{\epsilon_{r,m}\epsilon_0}\left[1 + (1-q)\frac{F\phi_m}{RT}\right]^{\frac{1}{1-q}}, \quad r_0 < r < r_0 + d \quad (13)$$

where q is the so-called Tsallis entropic parameter.[40,41] In the limit $q \to 0$, the counterions (the electrolyte anions in eq 13) are frozen within the monolayer, although in the opposite limit $q \to 1$ the diffuse P−B approach is regained (the q-exponential function becomes the exponential distribution for the counterions in the P−B equation of eq 13). Note that because q incorporates now part of the details of the monolayer, the partition coefficient $K < 1$ should attain now significantly higher values than those assumed in the above figures where the above details were implicitly lumped into this free parameter.

Figure 12 shows the electric potential change $\Delta V = e/C_{MPC}$ vs z for the partition coefficient $K = 10^{-2}$ and the values of q in the figure. Other model parameters are $r_0 = 1$ nm, $d =$ 1 nm, $\epsilon_{r,m} = 4$, $\epsilon_{r,s} = 10$, and $c_s = 10$ mM. In the limit $q \to 1$ (dashed curve), we recover the case of the diffuse layer model considered in Figure 9. However, as q is gradually reduced down to zero, the case of a compact monolayer with no counterion motion is obtained. For intermediate values of q, a significant decrease of ΔV with z is predicted. The values $q < 1$ reflect the reduction in the phase space available[40] for the counterion within the monolayer and give more gradual changes of ΔV than those of Figure 9.

For low values of the electrostatic potential (low z), the right hand side of eq 13 can be linearized to give

$$\frac{FKc_s}{\epsilon_{r,m}\epsilon_0}\left[1+(1-q)\frac{F\phi_m}{RT}\right]^{1/1-q} \approx \frac{FKc_s}{\epsilon_{r,m}\epsilon_0}\left[1+\frac{F\phi_m}{RT}\right] \quad (14)$$

Note that in this limit there is no dependence on q (the effect of q is most significant for high surface potentials corresponding to high values of z in Figure 12). Therefore, K can be estimated by fitting separately the experimental results at low charge to the model results obtained from eq 13 with the rhs of eq 13 replaced by the approximation in eq 14. Once K is obtained using this procedure, the full eq 13 can be solved (with K fixed) to extract q from the experimental data at higher z. Parameter K should reflect the interaction between a single counterion and the nanoparticle while q reflects the collective electrostatic correlations that arise between the cloud of counterions and the metallic core at higher z as well as the monolayer structural details. In this simplified view of the problem, the structure of the monolayer influences both K and q.

Experimental values of $\Delta V = e/C_{MPC}$ for the electrolyte tetraphenylarsonium pentafluorophenyl borate ($TPAsTPBF_{20}$) in the solvent 1,2-dichloroethane (DCE) (circles), tetrabutylammonium hexafluorophosphate ($TBAPF_6$) in DCE (squares), and $TBAPF_6$ in chlorobenzene (CB) (triangles) are included in Figure 13 (see ref 27 for details). The theoretical curves are obtained with eq 13 as follows. First, the solution dielectric constants $\epsilon_{r,s} = 10.24$ (DCE) and 5.6 (CB), together with the geometrical characteristics $r_0 = 0.81$ nm, $d = 0.77$ nm, and $c_s = 10$ mM, are taken from ref 27. The potential change ΔV at zero charge is very sensitive to the dimensions of the protected nanocluster and the dielectric constants of the solvent and the monolayer (see eq 10 as well as Figure S1 in Supporting Information for the MPC capacitance). Assuming that the geometrical characteristics r_0 and d are the same for every experiment, the effective monolayer dielectric constants $\epsilon_{r,m}$ can be obtained from eq 10, which is valid in the limit $z = 0$ (see also Figure 3), and the experimental values of ΔV at $z = 0$. This procedure gives $\epsilon_{r,m} = 3.6$ ($TPAsTPBF_{20}$ in DCE, continuous curve), $\epsilon_{r,m} = 3.0$ ($TBAPF_6$ in DCE, dashed line), and $\epsilon_{r,m} = 2.3$ ($TBAPF_6$ in CB, dotted line). Subsequently, we obtain $K = 0$ (continuous curve), $K = 10^{-3}$ (dashed line), and $K = 7 \times 10^{-3}$ (dotted line) from the fitting of the experimental results at low charge to the capacitances obtained from the generalized P−B equation with the rhs of eq 13 replaced by the approximation in eq 14. Finally, parameter q is determined by using the full P−B equation in eq 13; the unique value $q = 0.79$ is valid for the theoretical curves of Figure 13. This may suggest that q reflects rather general collective properties, as opposed to K, which is a characteristic of each particular counterion, although the analysis is still too preliminary.

4. Conclusions

The predictions of the concentric sphere capacitor model have been critically analyzed over a broad range of experimental parameters concerning the MPC geometrical and electrostatic characteristics as well as the electrolyte solution properties. The theoretical approach employed is based on the P−B equation extended to account for ion penetration. The results obtained show that capacitance C_0 gives both the correct order of magnitude as well as some qualitative features of the total MPC capacitance C_{MPC}, although significant deviations are predicted for realistic values of r_0, d, z, $\epsilon_{r,m}$, c_s, and $\epsilon_{r,s}$, especially in those cases where ion and solvent penetration are important. These deviations are quantitatively important when attempting to determine the potential separation between quantized double layer charging events, $\Delta V = e/C_{MPC}$. A generalized P−B equation that considers the monolayer as a disordered medium where the thermal motion of the counterions is decreased because of electrostatic correlations and monolayer structural effects is proposed on the basis of the Tsallis q-exponential distribution, and model calculations are compared with recent experimental data. Admittedly, most of the results obtained are extensions of recent theoretical and experimental work,[25−27] but the addition of some new physical insights concerning the ion penetration problem may be useful for the understanding and future applications of the nanoparticle electrical properties.

Acknowledgment. Financial support from the CICYT, Ministerio de Ciencia y Tecnología (Project No. MAT2005-01441) and the European Union (project DYNAMO, program New Emerging Science and Technology) are acknowledged. We thank also Professor José A. Manzanares and two anonymous reviewers for helpful comments. This paper is dedicated to Professor Julio Pellicer on the occasion of his retirement.

Supporting Information Available: Additional theoretical results for the MPC capacitance as a function of the electrolyte solution concentration and MPC charge number are given. This material is available free of charge via the Internet at http://pubs.acs.org.

References and Notes

(1) Brust, M.; Walker, M.; Bethell, D.; Schifrin, D. J.; Kiely, R. *J. Chem. Soc., Chem. Commun.* **1994**, 801−802.
(2) Chen, S.; Ingram, R. S.; Hostetler, M. J.; Pietron, J. J.; Murray, R. W.; Schaaff, T. G.; Khoury, J. T.; Alvarez, M. M.; Whetten, R. L. *Science* **1998**, *280*, 2098−2101.
(3) Pietron, J. J.; Hicks, J. F.; Murray, R. W. *J. Am. Chem. Soc.* **1999**, *121*, 5565−5570.
(4) Templeton, A. C.; Wuelfing, W. P.; Murray, R. W. *Acc. Chem. Res* **2000**, *33*, 27−36.
(5) Chen, S.; Sommers, J. M. *J. Phys. Chem. B* **2001**, *105*, 8816−8820.
(6) Quinn, B. M.; Liljeroth, P.; Ruiz, V.; Laaksonen, T.; Kontturi, K. *J. Am. Chem. Soc.* **2003**, *125*, 6644−6645.
(7) Weaver, M. J.; Gao, X. *J. Phys. Chem.* **1993**, *97*, 332−338.
(8) Chen, S.; Murray, R. W.; Feldberg, S. W. *J. Phys. Chem. B* **1998**, *102*, 9898−9907.
(9) Hicks, J. F.; Templeton, A. C.; Chen, S.; Sheran, K. M.; Jasti, R.; Murray, R. W.; Debord, J.; Schaaff, T, G.; Whetten, R. L. *Anal. Chem.* **1999**, *71*, 3703−3711.
(10) Krcmar, M.; Saslow, W. M.; Zangwill, A. *Appl. Phys. Lett.* **2001**, *105*, 8979−8988.
(11) Cheng, W.; Dong, S.; Wang, E. *Electrochem. Commun.* **2002**, *4*, 412−416.
(12) Hicks, J. F.; Miles, D. T.; Murray, R. W. *J. Am. Chem. Soc.* **2002**, *124*, 13322−13328.
(13) Chaki, N. K.; Aslam, M.; Gopakumar, T. G.; Sharma, J.; Pasricha, R.; Mulla, I. S.; Vijayamohanan, K. *J. Phys. Chem. B* **2003**, *107*, 13567−13574.
(14) Chaki, N. K.; Gopakumar, T. G.; Maddanimath, T.; Aslam, M.; Vijayamohanan, K. P. *J. Appl. Phys.* **2003**, *94*, 3663−3665. (Erratum: *J. Appl. Phys.* **2003**, *94*, 7379).
(15) Li, D.; Li, J. *Chem. Phys. Lett.* **2003**, *372*, 668−673.
(16) Miles, D. T.; Murray, R. W. *Anal. Chem.* **2003**, *75*, 1251−1257.
(17) Miles, D. T.; Leopold, M. C.; Hicks, J. F.; Murray, R. W. *J. Electroanal. Chem.* **2003**, *554*, 87−97.
(18) Chaki, N. K.; Kakade, B.; Sharma, J.; Mahima, S.; Vijayamohanan, K. P.; Haram, S. K. *J. Appl. Phys.* **2004**, *96*, 5032−5036.
(19) Chaki, N. K.; Kakade, B.; Vijayamohanan, P. *Electrochem. Commun.* **2004**, *6*, 661−665.
(20) Cortie, M. B.; Zareie, M. H.; Ekanayake, S. R.; Ford, M. J. *IEEE Trans. Nanotechnology* **2005**, *4*, 406−414.
(21) Kim, Y.-G.; Garcia-Martinez, J. C.; Crooks, R. M. *Langmuir* **2005**, *21*, 5485−5491.
(22) Chaki, N. K.; Kakade, B.; Vijayamohanan, K. P.; Singh, P.; Dharmadhikari, C. V. *Phys. Chem. Chem. Phys.* **2006**, *8*, 1837−1844.
(23) Wolfe, R. L.; Murray, R. W. *Anal. Chem.* **2006**, *78*, 1167−1173.

(24) Branham, M. R.; Douglas, A. D.; Mills, A. J.; Tracy, J. B.; White, P. S.; Murray, R. W. *Langmuir* **2006**, *22*, 11376−11383.
(25) Su, B.; Zhang, M.; Shao, Y.; Girault, H. H. *J. Phys. Chem. B* **2006**, *110*, 21460−21466.
(26) Guo, R.; Georganopoulou, D.; Feldberg, S. W.; Donkers, R.; Murray, R. W. *Anal. Chem.* **2005**, *77*, 2662−2669.
(27) Laaksonen, T.; Pelliniemi, O.; Quinn, B. M. *J. Am. Chem. Soc.* **2006**, *128*, 14341−14346.
(28) Bard, A. J.; Faulkner, R. *Electrochemical Methods, Fundamentals and Applications*, 2nd ed.; John Wiley & Sons: New York, 2001.
(29) Su, B.; Girault, H. H. *J. Phys. Chem. B* **2005**, *109*, 11427−11431.
(30) Su, B.; Girault, H. H. *J. Phys. Chem. B* **2005**, *109*, 23925−23929.
(31) Ohshima, H. Electrical Double Layer. In *Electrical Phenomena at Interfaces: Fundamentals, Measurements and Applications*; Ohshima, H., Furusawa, K., Eds.; Marcel Dekker: New York, 1998; pp 1−18.
(32) Reimers, J. R.; Hush, N. S. *J. Phys. Chem. B* **2001**, *105*, 8979−8988.
(33) Muller, F.; Fontaine, P.; Delsanti, M.; Belloni, L.; Yang, J.; Chen, Y. J.; Mays, J. W.; Lesieur, P.; Tirrell, M.; Guenoun, P. *Eur. Phys. J. E* **2001**, *6*, 109−115.
(34) Rimer, J. D.; Lobo, R. F.; Vlachos, D. G. *Langmuir* **2005**, *21*, 8960−8971.
(35) Misra, S.; Varanasi, S. *J. Chem. Phys.* **1991**, *95*, 2183−2192.
(36) Fawcett, W. R.; Smagala, T. G. *Langmuir* **2006**, *22*, 10635−10642.
(37) Cervera, J.; Garcia-Morales, V.; Pellicer, J. *J. Phys. Chem. B* **2003**, *107*, 8300−8309.
(38) Garcia-Morales, V.; Cervera, J.; Pellicer, J. *Physica A* **2004**, *339*, 482−490.
(39) Garcia-Morales, V.; Cervera, J.; Pellicer, J. *Phys. Lett. A* **2005**, *336*, 82−88.
(40) Garcia-Morales, V.; Pellicer, J. *Physica A* **2006**, *361*, 161−172.
(41) Tsallis, C. *J. Stat. Phys.* **1988**, *52*, 479−487.